In vivo biodistribution and highly efficient tumour targeting of carbon nanotubes in mice

ZHUANG LIU[1]*, WEIBO CAI[2]*, LINA HE[2], NOZOMI NAKAYAMA[1], KAI CHEN[2], XIAOMING SUN[1], XIAOYUAN CHEN[2†] AND HONGJIE DAI[1†]

[1]Department of Chemistry, Stanford University, Stanford, California 94305, USA
[2]The Molecular Imaging Program at Stanford (MIPS), Department of Radiology and Bio-X Program, Stanford University School of Medicine, Stanford, California 94305, USA
*These authors contributed equally to this work
[†]e-mail: hdai@stanford.edu; shawchen@stanford.edu

Published online: 17 December 2006; doi:10.1038/nnano.2006.170

Single-walled carbon nanotubes (SWNTs) exhibit unique size, shape and physical properties[1–3] that make them promising candidates for biological applications. Here, we investigate the biodistribution of radio-labelled SWNTs in mice by *in vivo* positron emission tomography (PET), *ex vivo* biodistribution and Raman spectroscopy. It is found that SWNTs that are functionalized with phospholipids bearing polyethylene-glycol (PEG) are surprisingly stable *in vivo*. The effect of PEG chain length on the biodistribution and circulation of the SWNTs is studied. Effectively PEGylated SWNTs exhibit relatively long blood circulation times and low uptake by the reticuloendothelial system (RES). Efficient targeting of integrin positive tumour in mice is achieved with SWNTs coated with PEG chains linked to an arginine–glycine–aspartic acid (RGD) peptide. A high tumour accumulation is attributed to the multivalent effect of the SWNTs. The Raman signatures of SWNTs are used to directly probe the presence of nanotubes in mice tissues and confirm the radio-label-based results.

An emerging field in nanotechnology is the exploration of interesting structural, mechanical, electrical and optical properties of SWNTs[1–3] for biological applications including biosensors[4], molecular transporters for drug delivery[5–12] and potential new therapies[11]. Water-solubilized carbon nanotubes are found to traverse the cell membrane via endocytosis to deliver molecular cargoes including proteins[13] and nucleic acids such as plasmids[9] and short interfering RNA[10]. The intrinsic physical properties of SWNTs can also be exploited. The high optical absorbance of SWNTs in the near-infrared regime causes heating under laser irradiation, which is useful for destroying cancer cells that are selectively internalized with nanotubes[11]. Various groups have found that well water-solubilized nanotubes with high hydrophilicity are non-toxic, even at high concentrations[5–12,14,16].

The fate and biological effects of carbon nanotubes in animals are critical to potential applications *in vivo*. There are only two reports on the biodistribution of chemically functionalized nanotubes intravenously injected into animals[17,18]. In these, Wang *et al.*[17] and Singh *et al.*[18] reported that two differently functionalized SWNTs behaved like small molecules in mice and freely cleared through the urine with little uptake by the liver or other organs of the RES. It therefore appears, based on the information to date, that SWNTs defy the general trend of high RES uptake observed for nanomaterials in general[19,20]. The validity and generality of these results deserve careful investigation. Also, much effort is needed to achieve targeted accumulation of SWNTs *in vivo*, a goal central to potential therapeutics[19,20], which has not yet been achieved with nanotubes.

In this work, we investigated the biodistribution and tumour targeting ability of SWNTs in mice, using Hipco nanotubes non-covalently functionalized with phospholipid–PEG (PL–PEG), the PEG chains being one of two different lengths (molecular weight of PEG chains = 2,000 and 5,400, respectively) (Fig. 1a). The diameters and lengths of the PL–PEG-functionalized SWNTs were 1–5 nm and 100–300 nm, respectively (Fig. 1b) and were well solubilized and suspended in buffers and whole serum without any aggregation (Fig. 1c; also see Supplementary Information, Fig. S1). Macrocyclic chelating agent DOTA (1,4,7,10-tetraazacyclododecane-1,4,7,10-tetraacetic acid) was attached to the termini of the PEG chains and used to conjugate positron emitting radionuclide ^{64}Cu (radio decay half-life $t_{1/2} = 12.7$ h) (Fig. 1a). Owing to the importance of integrin $\alpha_v\beta_3$ to tumour angiogenesis and metastasis[21,22], we conjugated SWNTs to both ^{64}Cu and c(RGDyK) (Fig. 1a), a potent integrin $\alpha_v\beta_3$ antagonist, aimed at *in vivo* targeting of integrin $\alpha_v\beta_3$-positive tumours in mice via specific RGD–integrin $\alpha_v\beta_3$ binding[23,24]. We measured the numbers of DOTA (by isotope dilution assay[25]) and RGD conjugated to SWNTs (see Supplementary Information, Table S1), carried out a receptor binding assay, and observed the multivalent binding of SWNTs to cell-surface receptors via multiple RGD on each tube (see Supplementary Information, Fig. S4). Importantly, the ^{64}Cu radio labels remained intact on SWNTs after incubation in full mouse serum over 24 h (Fig. 1d). No detachment from nanotubes was observed owing to strong binding of the phospholipids onto SWNTs[10,11], even when heated to high temperatures, as demonstrated by the lack of nanotube aggregation at 70 °C over more than 1 week (see Supplementary Information, Fig. S1).

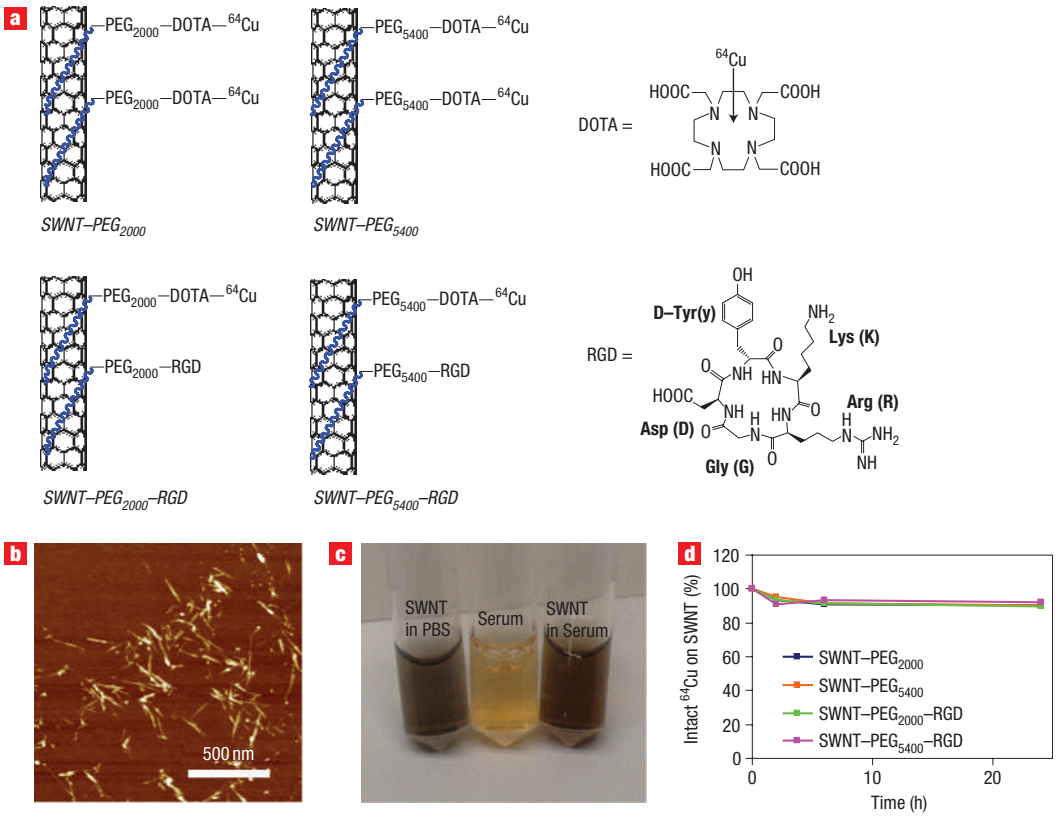

Figure 1 Water-soluble carbon nanotubes functionalized with PEG, radio labels and RGD peptide. a, Schematic drawings of non-covalently functionalized SWNT–PEG_{2000}, SWNT–PEG_{5400}, SWNT–PEG_{2000}–RGD, SWNT–PEG_{5400}–RGD with DOTA–^{64}Cu. The hydrophobic carbon chains (blue segments) of the phospholipids strongly bind to the sidewalls of the SWNTs, and the PEG chains render water solubility to the SWNTs. The DOTA molecules on the SWNTs are used to chelate ^{64}Cu for radio labelling. **b**, An atomic force microscope AFM image of SWNT–PEG_{5400} deposited on a silicon substrate. **c**, A photograph of stable SWNT–PEG_{2000} suspensions in PBS and full fetal bovine serum. **d**, Serum stability test showing that ^{64}Cu remains intact on carbon nanotubes over 24-h incubation in full mouse serum. The slight reduction during the early two time points was due to the removal of residual free ^{64}Cu radio labels in the nanotube solution by filtration.

Mice bearing subcutaneous integrin $\alpha_v\beta_3$-positive U87MG tumours were intravenously injected with SWNT–PEG_{2000} and SWNT–PEG_{5400}, followed by microPET scans at multiple time points (up to 24 h). Both SWNT conjugates exhibited prominent uptake in the liver (Fig. 2a, b), with lower uptake for SWNT–PEG_{5400} than SWNT–PEG_{2000} (Fig. 2b). Blood sampling revealed that SWNT–PEG_{5400} exhibited a much longer blood circulation time ($t_{1/2} \approx 2$ h) than SWNT–PEG_{2000} ($t_{1/2} \approx 0.5$ h) (Fig. 2c). Biodistribution in various organs (Fig. 3a) after killing the mice at 24 h post-injection (p.i.) revealed prominent SWNT uptake in the liver and spleen (consistent with PET data, Fig. 3c) and low uptake in the tumour, muscle, bone, skin and other organs.

The fact that much of the radioactivity remained in the mice at 24 h p.i. (Fig. 3d) suggested relatively slow excretion of SWNTs, which differed from the previous finding where SWNTs acted as small molecules, with little RES uptake and free excretion from mice[17,18]. Note that the dimensions of our SWNTs (diameter ~1–5 nm, length ~100–300 nm) were in fact smaller than the SWNT bundles (diameter ~10–40 nm, length ~1 μm or larger) used in previous reports[17,18]. It is known that RES uptake of nanomaterials is size-dependent and should be higher for larger sizes[20]. Our biodistribution data were accurate, because there were few free unconjugated ^{64}Cu radio labels in our SWNT solutions and the ^{64}Cu-conjugated SWNTs were serum stable (Fig. 1c, d). Otherwise, it is known that small molecules (such as free ^{64}Cu ions and PEG–^{64}Cu) would indeed be rapidly excreted from mice via the urine over several hours[26].

The biodistribution of our SWNTs is similar to other nanomaterials (sizes ~10–100 nm) with a tendency to undergo RES uptake, including in the liver[19,20]. RES uptake occurs via osponization, that is, antibody binding to nanomaterials in the plasma for recognition by phagocytes in the RES. We found that PEGylation by PL–PEG_{5400} imparted to SWNTs high hydrophilicity and resistance to protein nonspecific binding (NSB) (PL–PEG_{2000} functionalization was insufficient to prevent protein NSB to SWNTs; see Supplementary Information, Fig. S3), consistent with the reduced RES uptake and longer blood circulation of SWNT–PEG_{5400}[19,20].

Next, we show the efficient targeting of integrin $\alpha_v\beta_3$-positive U87MG tumours via RGD-functionalization of SWNT–PEG_{5400} and specific RGD–integrin $\alpha_v\beta_3$ recognition (Fig. 4, and see Fig. 3b for biodistribution of SWNT–PEG_{5400}–RGD). Although SWNT–PEG_{2000}–RGD showed only a slight increase in tumour uptake compared to that without RGD (Fig. 4a, first column and Fig. 4b), SWNT–PEG_{5400}–RGD exhibited a high tumour uptake of ~10–15% injected dose (ID) g^{-1} (Fig. 4a, second column), a significant increase from ~3–4% ID g^{-1} for SWNT–PEG_{5400} free of RGD (Fig. 4c). Tumour uptake of SWNTs was rapid, reaching a plateau at about 6 h p.i., and then levelled off in the next 20 h. The tumour uptake levels derived from PET images were

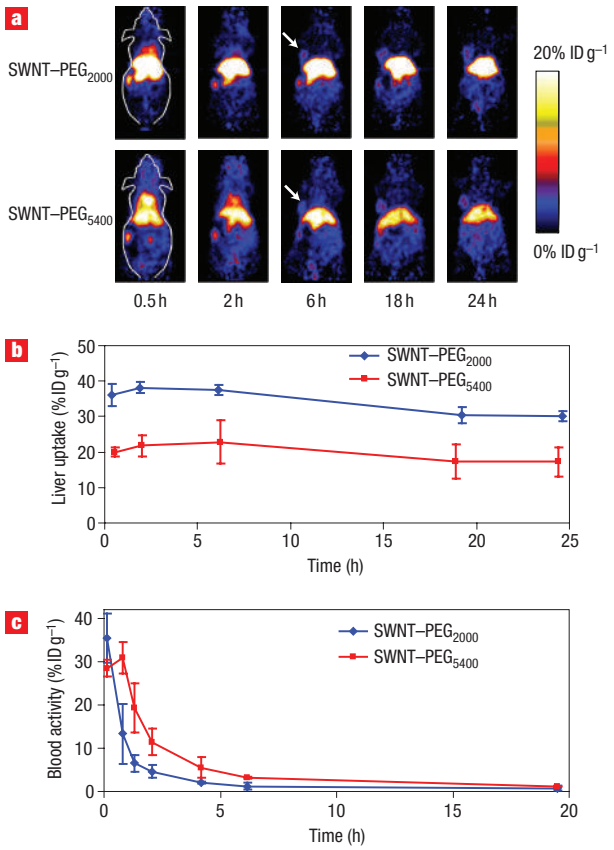

Figure 2 Functionalization-dependent biodistribution and blood circulation of intravenously injected SWNTs in mice bearing the U87MG human glioblastoma tumour. a, MicroPET images of two mice at various time points post tail-vein injection of ^{64}Cu-labelled SWNT–PEG$_{2000}$ and SWNT–PEG$_{5400}$, respectively. The arrows point to the tumours. **b**, Liver uptake curves over time as measured by PET for the two SWNT conjugates. **c**, Blood activity curves for the two conjugates. All data points represent three animals per group (four mice per group for **c**).

consistent with what was measured by biodistribution (Fig. 3b), and the tumour/muscle uptake ratio was calculated to be >15 for SWNT–PEG$_{5400}$–RGD. The high tumour accumulation was a result of the long blood circulation time, the specific high tumour-binding affinity of RGD-functionalized SWNT–PEG$_{5400}$, and the multivalency effect (that is, multiple RGDs along a SWNT binding to multiple integrin $\alpha_v\beta_3$ simultaneously; see Supplementary Information, Fig. S4). Note that without nanotubes, PEG–RGD–^{64}Cu species were known to be rapidly cleared from mice through the renal route in just a few hours, and U87MG tumour accumulation peaked at around ~3% ID g^{-1} 30 min after injection, and decreased afterwards[26]. In control experiments, we injected a blocking dose of c(RGDyK) (15 mg kg^{-1}) into U87MG tumour-bearing mice along with SWNT–PEG$_{5400}$–RGD, and observed that the uptake of nanotubes in the tumour was significantly blocked (Fig. 4a, third column). Mice bearing integrin $\alpha_v\beta_3$-negative HT-29 tumours (see Supplementary Information, Fig. S5) were also injected with SWNT–PEG$_{5400}$–RGD, and little tumour uptake of nanotubes was observed (~3% ID g^{-1}, Fig. 4a, fourth column).

To take advantage of the intrinsic optical properties of SWNTs, we used Raman spectroscopy to directly detect SWNTs in the various tissues of a mouse. Non-covalently functionalized SWNTs exhibit strong resonance Raman bands, including the G band at ~1,580 cm^{-1}, characteristic of graphitic carbon (Fig. 5a) (refs 1 and 2). A U87MG tumour-bearing mouse injected with a high dose of SWNT–PEG$_{5400}$–RGD (0.5 mg kg^{-1}) was killed after PET imaging (Fig. 5b) at 8 h p.i. Raman spectroscopy clearly revealed the existence of SWNTs in the liver and tumour samples with high G-band Raman intensities, a slight signal in the kidney sample, and no SWNT Raman signal in muscle (Fig. 5c). The amounts of SWNT in each of the tissue samples, derived from Raman intensities calibrated against SWNT solutions with known concentrations, were in reasonable agreement with PET data based on radioactivity of nanotubes (Fig. 5d). Thus, our Raman data provide direct proof of tumour uptake of SWNTs. The co-localization of ^{64}Cu radio labels and SWNTs in various mouse tissues also suggests a proof of the *in vivo* stability of our non-covalent functionalization of SWNTs. Such functionalization retains the intrinsic properties of SWNTs (for example, without the Raman intensity degradation seen in covalently modified tubes) for biological and medical applications such as Raman probing[27] and fluorescence imaging[8] *in vitro*, *ex vivo* and potentially *in vivo*.

We observed no obvious toxicity or negative health effects (such as weight loss and fatigue), with many mice injected with SWNT–PEG at dosages up to 2 mg kg^{-1} over monitoring periods of up to several months. However, the long-term fate of SWNT–PEG injected into mice requires further investigation. Based on the retained radioactivity in mice, we observed relatively slow excretion of SWNTs. Longer-term monitoring is currently ongoing to investigate SWNT clearance from mice.

Our current work establishes strong non-covalently functionalized SWNTs for *in vivo* applications. Surveying the literature, we found that the nanotube tumour accumulation of ~13% ID g^{-1} over long periods (>24 h) is among the best achieved using nanomaterials. The unique one-dimensional shape and flexible structure of SWNTs enables a polyvalency effect (see Supplementary Information, Fig. S4) and enhances tumour binding affinity. The one-dimensional shape may also facilitate SWNTs leaking out from blood microvessels to reach cancer cells in the tumour through vascular and interstitial barriers[28]. The exact distribution of our SWNTs within the tumour requires further investigation. SWNTs of various lengths will be ideal vehicles for elucidating size and shape effects on nanomaterial distribution within tumours. These discoveries will be useful for the application of the structural and physical properties of SWNTs for therapeutic approaches.

METHODS

PREPARATION OF PEGYLATED SWNTs

Raw Hipco SWNTs were sonicated in an aqueous solution of PL–PEG$_{2000}$–NH$_2$, that is, DSPE–PEG$_{2000}$–Amine (1,2-distearoyl-*sn*-glycero-3-phosphoethanolamine-N-(amino (polyethyleneglycol)2000)) (Avanti Polar Lipids) or PL–PEG$_{5400}$–NH$_2$, DSPE–PEG$_{5400}$–Amine for 1 h, centrifuged at 24,000 *g* for 6 h to obtain short, PL–PEG-functionalized SWNTs in supernatant. Filtration through 100-kDa filters (Millipore) removed excess phospholipids. PL–PEG$_{5400}$–NH$_2$ was synthesized by linking NHS–PEG$_{3400}$–Boc (Nektar) with PL–PEG$_{2000}$–NH$_2$ in aqueous solution followed by deprotection of Boc. The optical absorbance of the SWNTs was measured to determine their concentration (see Supplementary Information)[11].

DOTA AND RGD CONJUGATION TO SWNTs

DOTA–SNHS (Sulfo-NHS) was synthesized by reacting DOTA with *N*-hydroxysulphonosuccinimide in the presence of 1-ethyl-3-(3-(dimethylamino)-propyl) carbodiimide (EDC) at 1:1:1 molar ratio[29]. PL–PEG$_{2000}$–NH$_2$ and PL–PEG$_{5400}$–NH$_2$ functionalized SWNTs were mixed with DOTA–SNHS at pH 7.4 and incubated for 4 h. The SWNT solution was purified by filtration to remove unconjugated DOTA.

For conjugation of both RGD and DOTA, DOTA–SNHS and sulpho-SMCC (sulphosuccinimidyl 4-N-maleimidomethyl cyclohexane-1-carboxylate)

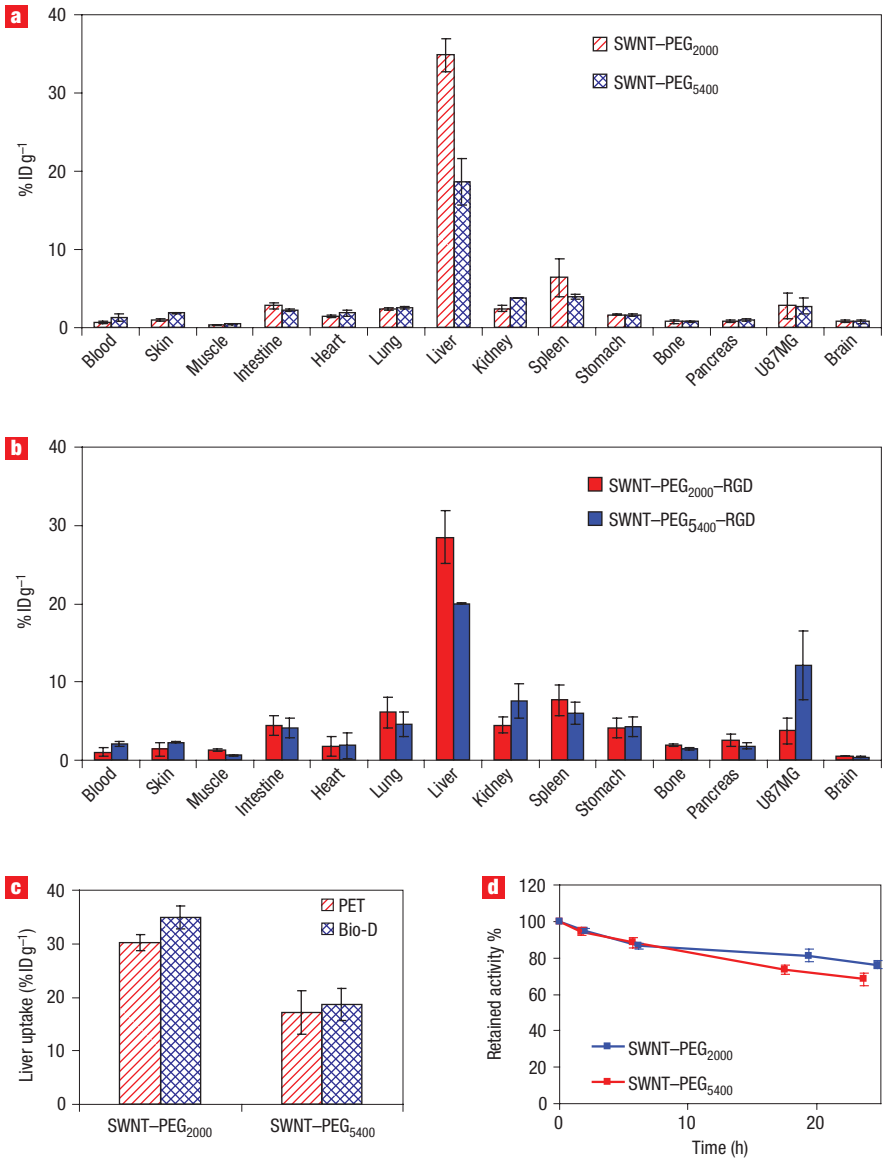

Figure 3 Biodistribution and retained activity of ^{64}Cu-labelled SWNTs in mice. **a**, Biodistribution of SWNT–PEG_{2000} and SWNT–PEG_{5400} in various organs at 24 h p.i. **b**, Biodistribution of SWNT–PEG_{2000}–RGD and SWNT–PEG_{5400}–RGD at 24 h p.i. **c**, Comparison of liver uptake of SWNTs measured by microPET and biodistribution at 24 h p.i. **d**, Total ^{64}Cu activity left in the mice at different time points p.i. of the two different SWNT conjugates. The radio-decay of ^{64}Cu with a half-life of 12.7 h was corrected in the data. All data shown are based on three mice per group.

were mixed at 1:5 molar ratios and incubated in SWNT–PEG–NH_2 solutions at pH 7.4 for 2 h. Upon removal of excess reagents, the SWNTs were reacted overnight with 0.2 mM of thiolated RGD[24] in the presence of 10 mM Tris(2-carboxyethyl) phosphine hydrochloride (TCEP) at pH 7.4, yielding SWNT–PEG_{2000}–RGD and SWNT–PEG_{5400}–RGD with both RGD and DOTA on the SWNTs.

^{64}Cu-LABELLING OF SWNTs AND SERUM STABILITY TEST

$^{64}CuCl_2$ (supplied by the University of Wisconsin-Madison) was diluted in 300 μl of 0.1 M sodium acetate buffer (NaOAc, pH 6.5). Two mCi of ^{64}Cu was added to 100 μl of each of the SWNT conjugates (~150 nM) buffered by 300 μl of 0.1 M NaOAc solution (pH 6.5). The reaction mixture was incubated for 1 h at 40 °C after which excess unconjugated ^{64}Cu was removed. The final radio-labelling yield was 60–80%.

The serum stability of radio labels on SWNTs was investigated by incubating ^{64}Cu-labelled SWNTs in full mouse serum at 37 °C for up to 24 h. Portions of SWNT–serum suspension were collected at different time points and filtered through 300-kDa cutoff filters. The filtrates were collected and the radioactivity was measured. The percentages of retained (intact) ^{64}Cu on the SWNTs were calculated by using the relation (total activity−activity in filtrate)/total activity.

CELL LINES AND THE ANIMAL MODEL

U87MG human glioblastoma and HT-29 human colorectal cancer cell lines (from American Type Culture Collection, ATCC) were cultured under standard conditions. The U87MG and HT-29 tumour models were generated by subcutaneous injection of 5×10^6 cells in 50 μl PBS into the front left and front right legs of the mice, respectively. The mice were used for the study when the tumour volume reached 200–300 mm^3.

MICROPET IMAGING

PET imaging was carried out on a microPET R4 rodent model scanner (Concorde Microsystems)[30]. About 1 μg of SWNTs (~30 nM) in 150–200 μl PBS with 200–300 μCi of ^{64}Cu were injected into each mouse at the tail vein,

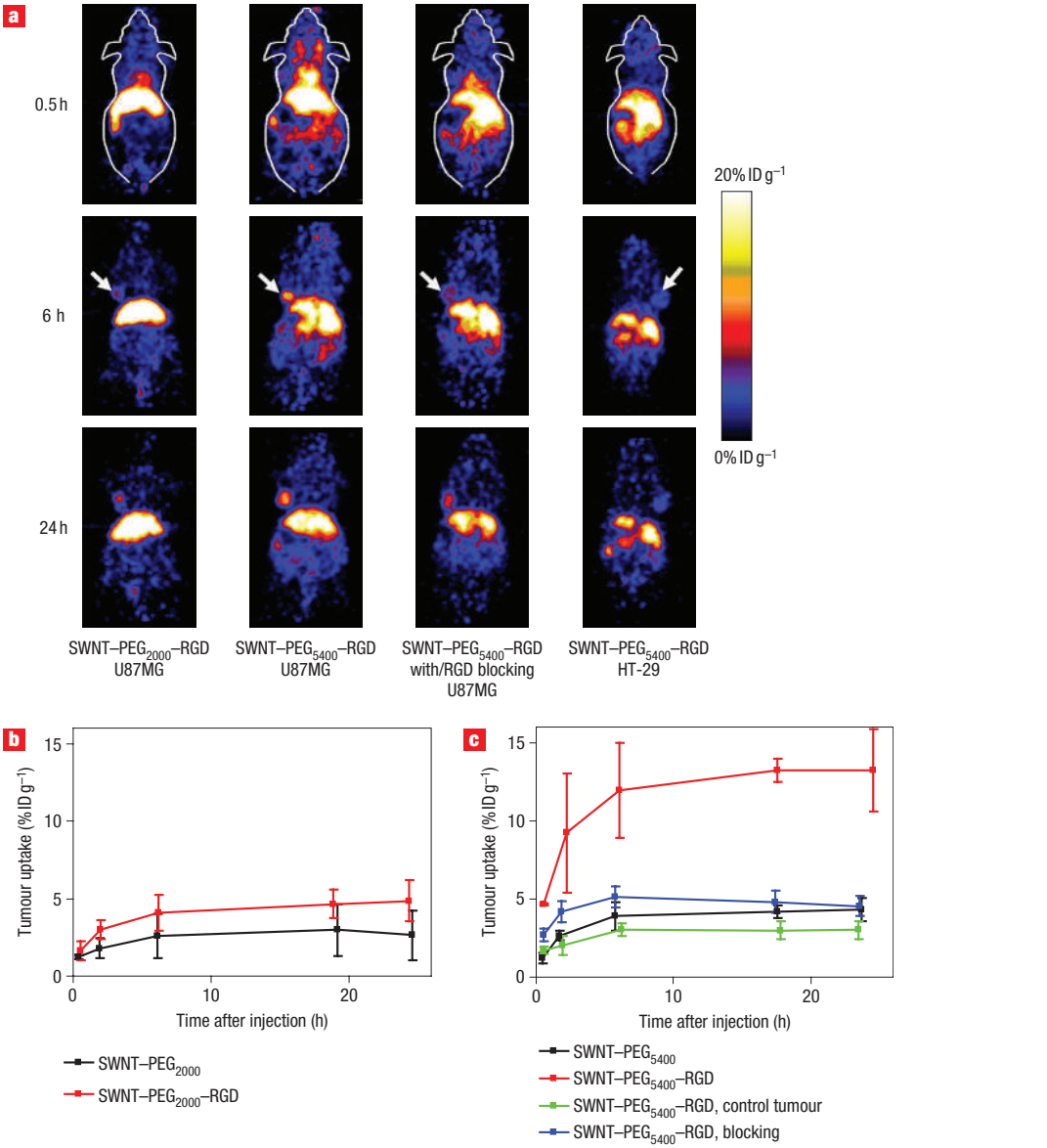

Figure 4 Targeting of integrin $\alpha_v\beta_3$-positive U87MG tumour in mice by RGD-functionalized SWNTs. a, MicroPET images of mice. The arrows point to the tumours. High tumour uptake (~15% ID g^{-1}) of SWNT–PEG_{5400}–RGD is observed in the U87MG tumour (second column), in contrast to the low tumour uptake (first column) of SWNT–PEG_{2000}–RGD. The third column is a control experiment showing blocking of SWNT–PEG_{5400}–RGD tumour uptake by co-injection of free c(RGDyK). The fourth column is a control experiment showing low uptake of SWNT–PEG_{5400}–RGD in an integrin $\alpha_v\beta_3$-negative HT-29 tumour. **b**,**c**, U87MG tumour uptake curves for mice injected with SWNT–PEG_{2000} (**b**) and SWNT–PEG_{5400} (**c**), with and without RGD. All data shown represent three mice per group.

except for one mouse, which was injected with ~10 μg of SWNTs for the Raman study. The tissue/organ uptake (% ID g^{-1}) based on PET imaging was calculated as described previously[25,30]. Note that all the PET data and biodistribution data have been decay corrected by the half-life of ^{64}Cu. Three mice in each group were used for the data presented in this work.

BIODISTRIBUTION AND BLOOD CIRCULATION STUDIES

Nude mice bearing U87MG tumours were injected with ~200–300 μCi of ^{64}Cu-labelled SWNTs. The mice were killed at 24 h p.i. The major organs were collected and wet weighed. The radioactivity in the tissues was measured using a γ-counter (Packard). For each mouse, the radioactivity of the tissue samples was calibrated against a known aliquot of the injectate, and normalized to a body weight of 25 g. Data presented were from three animals per group.

Approximately 3–5 μl of blood was taken from the tail vein of the mice injected with 200–300 μCi of ^{64}Cu-labelled SWNTs at different time points p.i., and the radioactivity was measured by a γ-counter. The data shown were based on four mice in each group. The values of blood circulation half-life were obtained by first-order exponential decay fits.

EX VIVO RAMAN SPECTROSCOPIC MEASUREMENTS OF MOUSE TISSUES

A U87MG tumour-bearing mouse injected with a high dose of SWNT–PEG_{5400}–RGD (0.05 mg ml^{-1}, 300 nM in 200 μl PBS) was killed at 8 h p.i. The tumour, liver, kidney and a portion of the muscle were lyophilized and sonicated in 1% SDS and 1% Triton X-100 solution to form homogenous suspensions. Raman spectra of the suspensions were acquired with a Renishaw micro-Raman instrument. SWNT suspensions in lysis buffer with known concentrations were measured to obtain a standard calibration curve (see Supplementary Information, Fig. S6), against which the SWNT concentrations in the tissue samples were calculated and compared to the microPET data. More experimental details can be found in the Supplementary Information.

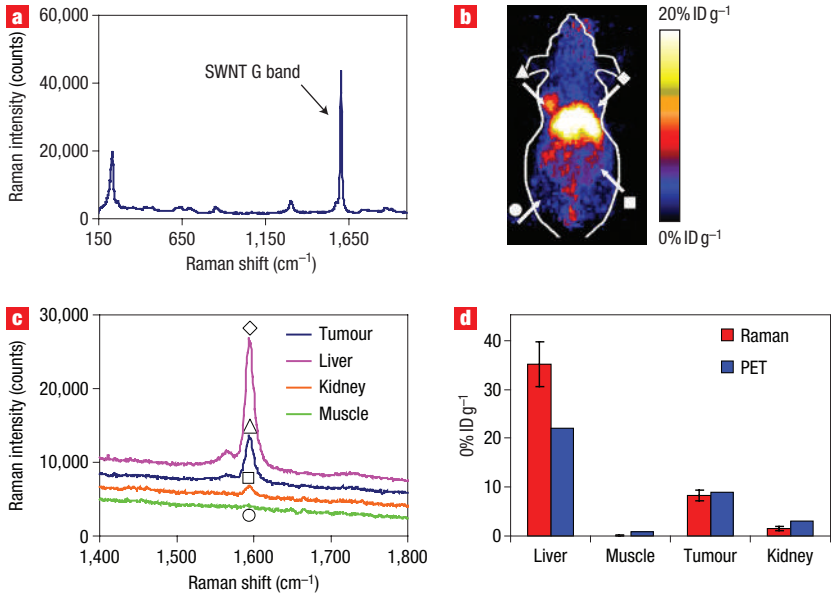

Figure 5 Detecting nanotubes in mice tissues using characteristic Raman signatures of SWNTs. a, A Raman spectrum of a solution of SWNT–PEG_{5400}. The G band of the SWNTs is indicated by the arrow. The peak at the lower Raman shift near 230 cm^{-1} corresponds to the radial breathing modes of the SWNTs. **b**, A two-dimensional projection of the microPET image of a U87MG tumour-bearing mouse 8 h p.i. of a high dose of SWNT–PEG_{5400}–RGD solution. The arrows point to the tumour and several organs used for Raman measurements (symbols correspond with those in **c**). **c**, Raman spectra in the G-band region of SWNTs recorded on lyophilized tumour and tissue powder samples suspended in surfactant solutions. The data provides direct evidence of the existence of SWNTs in the tumour. **d**, Comparison of the biodistribution data obtained by PET imaging and *ex vivo* Raman measurements. The error bars in the Raman data were obtained with several measurements performed over different parts of the tissues.

Received 15 September 2006; accepted 20 November 2006; published 17 December 2006.

References

1. Dresselhaus, M. & Dai, H. (eds) MRS 2004 *Carbon Nanotube Special Issue* (2004).
2. Dresselhaus, M. S., Dresselhaus, G. & Avouris, P. (eds) *Carbon Nanotubes* (Springer, Berlin, 2001).
3. Dai, H. Carbon nanotubes: opportunities and challenges. *Surf. Sci.* **500,** 218–241 (2002).
4. Chen, R. J. *et al.* Noncovalent functionalization of carbon nanotubes for highly specific electronic biosensors. *Proc. Natl Acad. Sci. USA* **100,** 4984–4989 (2003).
5. Kam, N. W. S., Jessop, T. C., Wender, P. A. & Dai, H. J. Nanotube molecular transporters: Internalization of carbon nanotube–protein conjugates into mammalian cells. *J. Am. Chem. Soc.* **126,** 6850–6851 (2004).
6. Pantarotto, D., Briand, J., Prato, M. & Bianco, A. Translocation of bioactive peptides across cell membranes by carbon nanotubes. *Chem. Commun.* 16–17 (2004).
7. Bianco, A., Kostarelos, K., Partidos, C. D. & Prato, M. Biomedical applications of functionalised carbon nanotubes. *Chem. Commun.* 571–577 (2005).
8. Cherukuri, P., Bachilo, S. M., Litovsky, S. H. & Weisman, R. B. Near-infrared fluorescence microscopy of single-walled carbon nanotubes in phagocytic cells. *J. Am. Chem. Soc.* **126,** 15638–15639 (2004).
9. Liu, Y. *et al.* Polyethylenimine-grafted multiwalled carbon nanotubes for secure noncovalent immobilization and efficient delivery of DNA. *Angew. Chem. Int. Edn Engl.* **44,** 4782 (2005).
10. Kam, N. W. S., Liu, Z. & Dai, H. Functionalization of carbon nanotubes via cleavable disulfide bonds for efficient intracellular delivery of siRNA and potent gene silencing. *J. Am. Chem. Soc.* **127,** 12492–12493 (2005).
11. Kam, N. W. S., O'Connell, M., Wisdom, J. A. & Dai, H. Carbon nanotubes as multifunctional biological transporters and near-infrared agents for selective cancer cell destruction. *Proc. Natl Acad. Sci. USA* **102,** 11600–11605 (2005).
12. Kam, N. W. S., Liu, Z. & Dai, H. J. Carbon nanotubes as intracellular transporters for proteins and DNA: An investigation of the uptake mechanism and pathway. *Angew. Chem. Int. Edn Engl.* **45,** 577–581 (2005).
13. Kam, N. W. S. & Dai, H. Carbon nanotubes as intracellular protein transporters: Generality and biological functionality. *J. Am. Chem. Soc.* **127,** 6021–6026 (2005).
14. Sayes, C. M. *et al.* Functionalization density dependence of single-walled carbon nanotubes cytotoxicity in vitro. *Toxicity Lett.* **161,** 135–142 (2006).
15. Chen, X. *et al.* Interfacing carbon nanotubes with living cells. *J. Am. Chem. Soc.* **128,** 6292–6293 (2006).
16. Dumortier, H. *et al.* Functionalized carbon nanotubes are non-cytotoxic and preserve the functionality of primary immune cells. *Nano Lett.* **6,** 1522–1528 (2006).
17. Wang, H. F. *et al.* Biodistribution of carbon single-wall carbon nanotubes in mice. *J. Nanosci. Nanotechnol.* **4,** 1019–1024 (2004).
18. Singh, R. *et al.* Tissue biodistribution and blood clearance rates of intravenously administered carbon nanotube radiotracers. *Proc. Natl Acad. Sci. USA* **103,** 3357–3362 (2006).
19. Moghimi, S. M., Hunter, A. C. & Murray, J. C. Long-circulating and target-specific nanoparticles: Theory to practice. *Pharmacol. Rev.* **53,** 283–318 (2001).
20. Moghimi, S. M., Hunter, A. C. & Murray, J. C. Nanomedicine: current status and future prospects. *FASEB J.* **19,** 311–330 (2005).
21. Mizejewski, G. J. Role of integrins in cancer: Survey of expression patterns. *Proc. Soc. Exp. Biol. Med.* **222,** 124–138 (1999).
22. Jin, H. & Varner, J. Integrins: Roles in cancer development and as treatment targets. *Br. J. Cancer* **90,** 561–565 (2004).
23. Xiong, J. P. *et al.* Crystal structure of the extracellular segment of integrin $\alpha_v\beta_3$ in complex with an Arg-Gly-Asp ligand. *Science* **296,** 151 (2002).
24. Cai, W. *et al.* Peptide-labeled near-infrared quantum dots for imaging tumor vasculature in living subjects. *Nano Lett.* **6,** 669–676 (2006).
25. Cai, W. *et al.* In vitro and in vivo characterization of ^{64}Cu-labeled Abegrin™, a humanized monoclonal antibody against integrin $\alpha_v\beta_3$. *Cancer Res.* **66,** 9673 (2006).
26. Chen, X. *et al.* Pegylated Arg-Gly-Asp peptide: ^{64}Cu labeling and PET imaging of brain tumor $\alpha_v\beta_3$-integrin expression. *J. Nucl. Med.* **45,** 1776–1783 (2004).
27. Heller, D. A., Baik, S., Eurell, T. E. & Strano, M. S. Single-walled carbon nanotube spectroscopy in live cells: Towards long-term labels and optical sensors. *Adv. Mater.* **17,** 2793–2799 (2005).
28. Jain, R. K. Vascular and interstital barriers to delivery of therapeutic agents in tumors. *Cancer Metastasis Rev.* **9,** 253–266 (1990).
29. Wu, Y. *et al.* MicroPET imaging of glioma integrin $\alpha_v\beta_3$ expression using ^{64}Cu-labeled tetrameric RGD peptide. *J. Nucl. Med.* **46,** 1707–1718 (2005).
30. Cai, W., Zhang, X., Wu, Y. & Chen, X. A thiol-reactive ^{18}F-labeling agent, N-[2-(4-^{18}F-fluorobenzamido)ethyl]maleimide (^{18}F-FBEM), and the synthesis of RGD peptide-based tracer for PET imaging of $\alpha_v\beta_3$ integrin expression. *J. Nucl. Med.* **47,** 1172–1180. (2006).

Acknowledgements

This work was supported in part by a Ludwig Translational Research Grant at Stanford University and NIH-NCI CCNE-TR at Stanford (H.D.), National Institute of Biomedical Imaging and Bioengineering (NIBIB) (R21 EB001785), National Cancer Institute (NCI) (R21 CA102123, P50 CA114747, U54 CA119367, R24 CA93862), Department of Defense (DOD) (W81XWH-04-1-0697, W81XWH-06-1-0665, W81XWH-06-1-0042, DAMD17-03-1-0143) and a Benedict Cassen Postdoctoral Fellowship from the Education and Research Foundation of the Society of Nuclear Medicine (to W.C.).
Correspondence and requests for materials should be addressed to H.D.
Supplementary information accompanies this paper on www.nature.com/naturenanotechnology.

Author contributions

H.D., X.C., Z.L. and W.C. conceived and designed the experiments. Z.L., W.C., X.C., L.H., N.N., K.C. and X.S. performed the experiments. H.D., Z.L., W.C. and X.C. co-wrote the manuscript.
All authors discussed the results and commented on the manuscript.

Competing financial interests

The authors declare that they have no competing financial interests.

NNANO-06090419A

Supplementary information

In-vivo biodistribution and highly efficient tumor targeting of carbon nanotubes in mice

Zhuang Liu[*1], Weibo Cai[*2], Lina He[2], Nozomi Nakayama[1], Kai Chen[2], Xiaoming Sun[1], Xiaoyuan Chen[†2], Hongjie Dai[†1]

[1]Department of Chemistry, Stanford University, Stanford, CA 94305, USA.
[2]The Molecular Imaging Program at Stanford (MIPS), Department of Radiology and Bio-X Program, Stanford University School of Medicine, Stanford, CA 94305, USA

* Contributed equally to this work

† Correspondence should be sent to: hdai@stanford.edu; shawchen@stanford.edu

Contents:

1. Comparison of aqueous stability of SWNTs functionalized by various methods

Phospholipid (PL)-PEG (PEG M.W. 2000 Da or 5400 Da) and sodium dodecyl sulfate (SDS) suspended SWNTs were made by sonicating raw Hipco SWNTs in aqueous solution of PL-PEG-NH_2 (1 mg/ml) or SDS (10 mg/lml) for 1 h followed by centrifugation at 24,000 g for 6 h to remove aggregates. Excess PL-PEG-NH_2 or SDS in the supernatant was removed by repeated filtration through 100 kDa filters and re-suspension in water. Hydroxylated SWNTs (SWNTols) were prepared following the method reported by Wang et al.[1]. In brief, SWNTs were mixed with KOH and agitated vigorously with the help of small stainless steel balls for 1 h at room temperature (r.t.). Then the SWNTols were dissolved in distilled water and centrifuged at 12,000 g for 15 min. Excess KOH was removed by filtration using 100 kDa filters.

PL-PEG-NH_2 suspended SWNTs are the most stable without any visible aggregation in water and phosphate buffered saline (PBS) after removing excess amount of free PL-PEG-NH_2 molecules. The nanotubes are stable in PBS without aggregation even after heating at 70 °C for one week (Fig. S1a, 1st row), suggesting no detachment of the coating under such harsh condition. SDS, a commonly used surfactant, can also be used to solubilize SWNTs, giving a good suspension in water. However, SDS suspended SWNTs are not stable in the absence of free SDS (Supplementary Fig. 1a, 2nd row), suggesting that the binding between SDS and SWNTs is not sufficiently strong. The in vivo biodistribution study of hydroxylated SWNTs (SWNTols) has been previously performed before by Wang et al.[1] However, this type of SWNTs is not very stable in PBS buffer. Obvious aggregation of SWNTols was seen after incubation in PBS overnight at either room temperature or 70 °C (Fig. S1 3rd row).

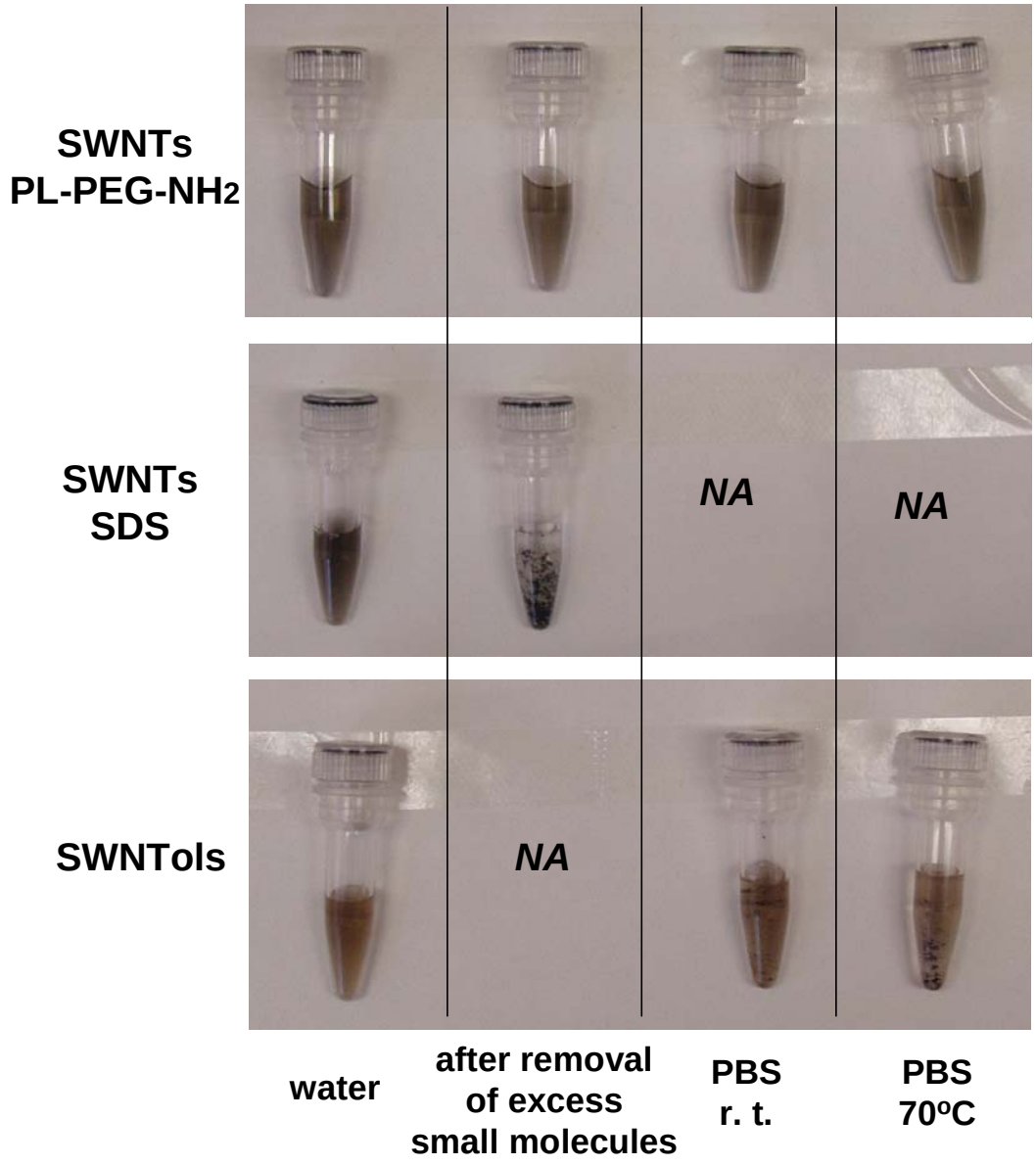

Figure S1. Stability of SWNTs functionalized by various methods. First row, phospholipid-PEG (PL-PEG-NH_2) suspended SWNTs are stable at all conditions, even at 70 °C for one week (the fourth photo). Second row, SDS suspended SWNTs are not stable after removal of excess SDS molecules in aqueous solution. Third row, hydroxylated SWNTs (SWNTols) aggregate in PBS buffer after overnight incubation at either room temperature or 70 °C (the third and fourth photo, respectively).

2. Measurement of SWNT concentration by UV-VIS-NIR spectroscopy

PL-PEG-NH_2 functionalized SWNTs exhibit high optical absorbance from

ultraviolet (UV) to near infrared (NIR) regimes (Fig.S2). The absorbance spectrum of a SWNT solution can be utilized to estimate the concentration of nanotubes[2]. The absorbance at 808 nm exhibits a molar extension coefficient of 7.9×10^6 $M^{-1} \cdot cm^{-1}$ for SWNTs with average length of ~200nm.[2]

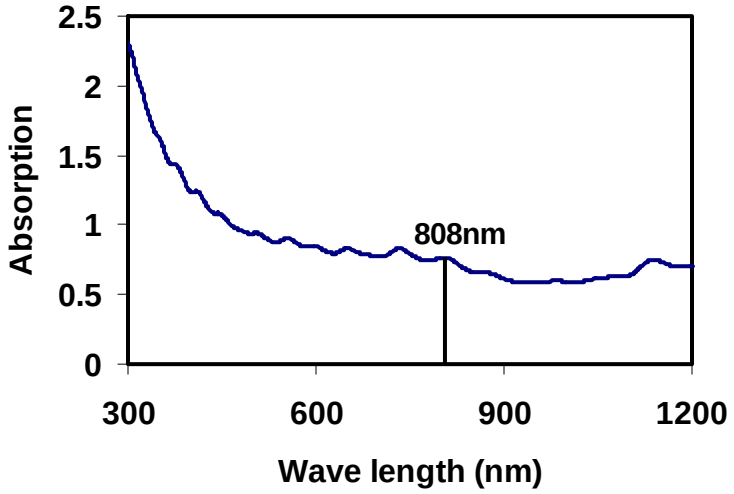

Fig. S2. A UV-VIS-NIR spectrum of SWNTs functionalized by PL-PEG-NH_2.

3. Number of DOTA and RGD peptides on the SWNTs

For SWNT-PEG_{2000} and SWNT-PEG_{5400} with and without conjugated RGD, the average number of DOTA chelators per SWNT was measured using a previously reported procedure with slight modifications.[3] Briefly, a defined amount of non-radioactive $CuCl_2$ (~150 fold excess of SWNT concentration) in 40 µl 0.1 M NaOAc buffer (pH = 6.5) was added to 0.2 mCi of $^{64}CuCl_2$ in 20 µl 0.1 M NaOAc buffer. Twenty µl of each SWNT conjugate in 100 µl 0.1 M NaOAc buffer was added to the above carrier-added $^{64}CuCl_2$ solution. The reaction mixtures were incubated with constant shaking at 40 ˚C for 1 h. ^{64}Cu-labeled SWNTs were purified using 100 kDa filters and the radio-labeling yield was calculated by measuring the radio activity retained in the

SWNTs solution. The number of DOTA per SWNT (average length ~150 nm) was determined as moles(Cu^{2+}) × yield/moles(SWNT).

	Average number of DOTA per SWNT	Std.
SWNT-PEG_{2000}	75.5	9.3
SWNT-PEG_{5400}	61.9	0.6
SWNT-PEG_{2000}-RGD	47.4	6.4
SWNT-PEG_{5400}-RGD	36.2	4.5

Supplementary Table 1. DOTA number assay. Standard deviations (std.) were obtained from 4 parallel samples.

The measured numbers of DOTA per nanotube of SWNTs with RGD conjugation (SWNT-PEG_{2000}-RGD and SWNT-PEG_{5400}-RGD) are less than those without RGD (SWNT-PEG_{2000} and SWNT-PEG_{5400}). Assuming 100% yield of thiolated RGD conjugation (a large excess of thiolated RGD was used), the ratio between RGD and DOTA on nanotubes will be 0.59:1 for SWNT-PEG_{2000}-RGD and 0.71:1 for SWNT-PEG_{5400}-RGD as calculated by the following equation:

[# of RGD per SWNT-PEG-RGD]/[# of DOTA per SWNT-PEG-RGD]=([# of DOTA per SWNT-PEG] – [# of DOTA per SWNT-PEG-RGD]) / [# of DOTA per SWNT-PEG-RGD]).

4. Non-specific binding (NSB) of SWNTs functionalized with different length PEGs

Ex vivo, we found that PEGylation by PL-PEG_{5400} imparted to SWNTs high hydrophilicity and resistance to protein NSB. PL-PEG_{2000} functionalization was insufficient to prevent protein NSB to SWNTs.

Four hundred nanoliter of mouse IgG (MIgG) solution was spotted on a

polylysine coated glass slide (Electron Microscopy Sciences) and allowed to dry. The glass slide was then rinsed briefly with PBS at pH 7.4 and subsequently blocked with 0.5 % tween20 and 3 % fetal bovine serum in PBS overnight. After blocking, the slide was rinsed briefly with PBS and water followed by drying with blowing air. Fourty nanomolar of SWNT-PEG_{2000} and SWNT-PEG_{5400} solution were dropped over the MIgG spots and allowed to incubate for 1 hr. After incubation, the slide was soaked in PBS for 30 min and then briefly rinsed with water before blow drying. Raman spectrum was taken at different positions inside the MIgG spot (~10mW power, 50 × objective, laser spot size ~2 μm^2, 30 s scan) and the averaged spectrums were presented in Fig. S3. The NSB level of SWNTs on substrates was determined based on the intensity of SWNT Raman G band peak.

SWNTs coated with PEG_{2000} exhibited appreciable NSB on MIgG spots on substrates, indicating the SWNTs sidewalls were not densely covered by hydrophilic PEG chains. In contrast, SWNTs coated with PEG_{5400} showed little NSB on MIgG spots, suggesting that the longer length of PEG_{5400} afforded sufficient hydrophilicity and biological inertness to SWNTs. The lower NSB of SWNTs coated with PEG_{5400} was consistent with the in-vivo behavior of lower liver uptake and longer circulation half-life.

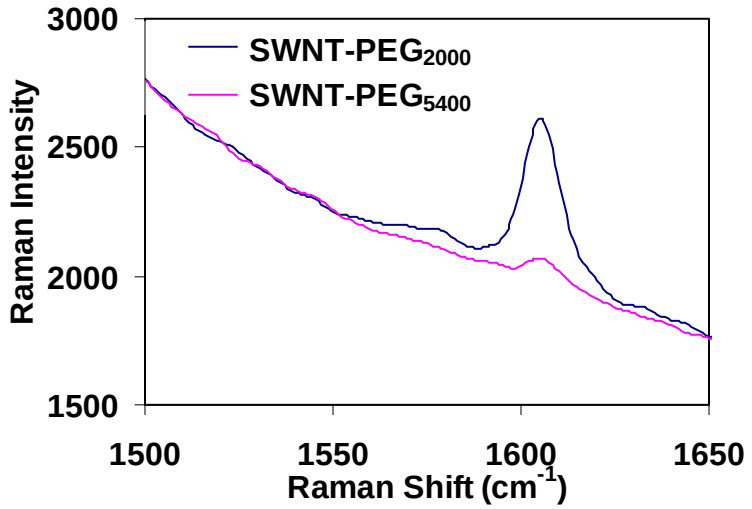

Fig. S3. Non-specific binding (NSB) of SWNTs with different PEG lengths. SWNT-PEG_{5400} has significantly lower NSB on mouse IgG protein substrate than SWNT-PEG_{2000}.

We suggest that the optimum length of PEG on SWNTs to impart high hydrophilicity and minimize NSB of proteins and antibodies (ex vivo and in vivo) will depend on the density of PEG chains on the tubes. For the particular phospholipid approach used in the current work, the packing of lipids on SWNT sidewalls may not be dense and long PEG_{5400} chains of the lipids are needed to impart sufficient hydrophilicity and NSB resistance. For denser PEGylation on SWNT sidewalls by other means, it is possible much shorter PEG can afford excellent inertness of SWNTs in vivo. Much remains to be done in developing such chemistry for nanotubes.

5. Receptor binding assay of SWNT-PEG-RGD

The in vitro integrin $\alpha_v\beta_3$-binding affinity and specificity of SWNT-PEG_{2000}-RGD and SWNT-PEG_{5400}-RGD were assessed via competitive displacement cell-binding assays using ^{125}I-echistatin as the $\alpha_v\beta_3$ integrin-specific radio-ligand [4]. Experiments were

performed on integrin $\alpha_v\beta_3$-positive U87MG human glioblastoma cells. The cells were harvested, washed twice with PBS and re-suspended (2×10^6 cells/ml) in binding buffer (20 mM Tris, pH 7.4, 150 mM NaCl, 2 mM $CaCl_2$, 1 mM $MgCl_2$, 1 mM $MnCl_2$, 0.1% BSA). Filter multiscreen DV plates (96-well, pore size: 0.65 μm, Millipore, Billerica, MA) were seeded with 1×10^5 cells per well and incubated with ^{125}I-echistatin (30,000 counts per minute (cpm)/well) in the presence of increasing concentrations of SWNT-PEG_{2000}-RGD or SWNT-PEG_{5400}-RGD (0 – 100 nM). The total incubation volume was adjusted to 200 μl. After the cells were incubated for 2 h at room temperature, the plates were filtered through a multi-screen vacuum manifold and washed twice with cold binding buffer. The hydrophilic polyvinylidene fluoride (PVDF) filters were collected and the radioactivity was determined using a gamma counter (Packard, Meriden, CT). The half maximal inhibitory concentration (IC_{50}) values were calculated by fitting the data by nonlinear regression using GraphPad Prism™ (GraphPad Software, Inc., San Diego, CA). Experiments were carried out twice with triplicate samples.

Echistatin is a viper venom disintegrin containing RGD loop which binds integrin $\alpha_v\beta_3$ with high affinity. The presence of SWNT-PEG-RGD can inhibit the binding between echistatin and integrin $\alpha_v\beta_3$ by competition, confirming the successful conjugation of RGD on SWNTs (Fig. S3). Both SWNT-PEG_{2000}-RGD and SWNT-PEG_{5400}-RGD inhibited the binding of ^{125}I-echistatin to $\alpha_v\beta_3$ integrin on U87MG cells, with IC_{50} values being 4.1 and 11.1 nM of SWNTs, respectively. The enhanced integrin $\alpha_v\beta_3$ binding affinity for the SWNT-PEG-RGD conjugates as compared to the monomeric RGD peptide ($IC_{50} = 67.9 \pm 6.1$ nM) [4] is likely due to the cooperative or multi-valent binding of multiple RGD units on the SWNT to multiple $\alpha_v\beta_3$ integrin, in accordance

with our previous findings that multimeric RGD peptides exhibit more potent binding to integrin $\alpha_v\beta_3$ than the monomeric peptide c(RGDyK) [4].

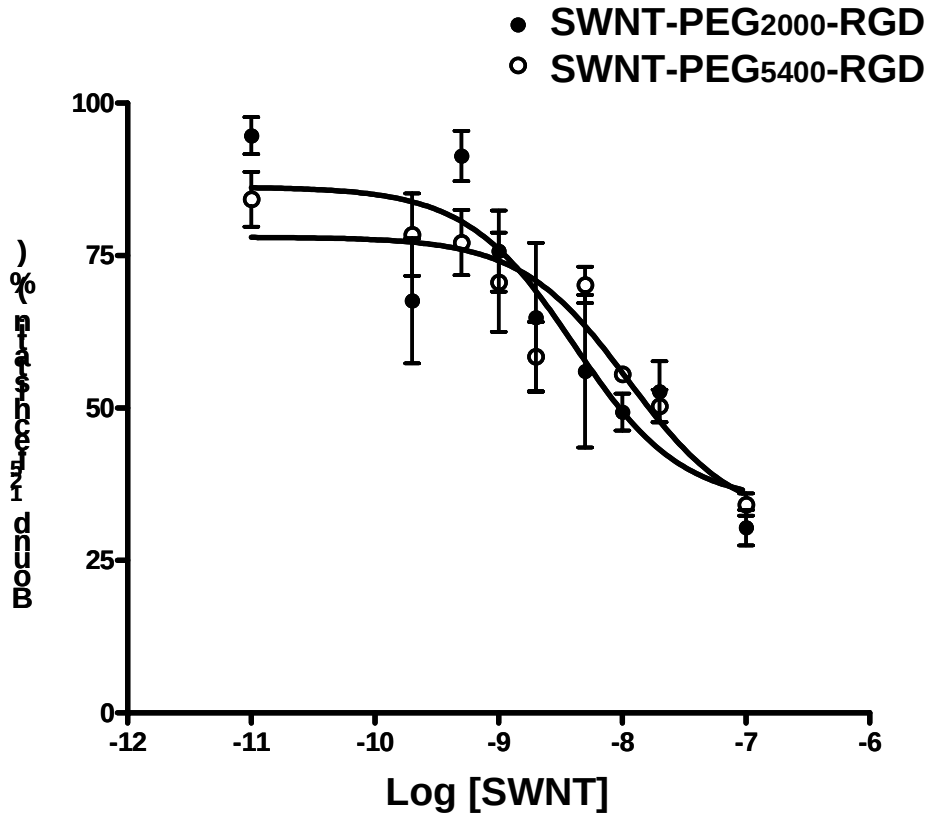

Fig. S4. Receptor binding assay. In vitro inhibition of ^{125}I-echistatin binding to $\alpha_v\beta_3$ integrin on U87MG human glioblastoma cells by SWNT-PEG$_{2000}$-RGD (●) and SWNT-PEG$_{5400}$-RGD (○), with IC_{50} values being 4.1 and 11.1 nM, respectively.

6. Immunofluorescence staining

Frozen tumor sections (5 μm) were warmed to room temperature, fixed with ice-cold acetone for 10 min, and dried in the air for 30 min. The sections were blocked with 10 % donkey serum for 1 hour at r.t.. For CD31 and human integrin $\alpha_v\beta_3$ double staining, the sections were incubated with rat anti-mouse CD31 (1:100, BD BioSciences, San Jose, CA) and Abegrin™ (anti-human integrin $\alpha_v\beta_3$ monoclonal antibody) (100 μg/mL) for 1

hour at r.t.. After incubating with Cy3-conjugated donkey anti-rat secondary antibody (1:200, Jackson ImmunoResearch Laboratories, Inc.) and FITC-conjugated donkey anti-human secondary antibody (1:200, Jackson ImmunoResearch Laboratories, Inc.), the tumor sections were examined under the microscope (Carl Zeiss Axiovert 200M, Carl Zeiss USA, Thornwood, NY). For CD31 and mouse integrin β_3 double staining, hamster anti-mouse β_3 (1:100, BD BioSciences) and FITC-conjugated goat anti-hamster secondary antibody (1:400, Jackson ImmunoResearch Laboratories, Inc) were used.

CD31 is a transmembrane glycoprotein highly expressed on endothelial cells but not on tumor cells. CD31 staining was performed to visualize tumor vasculature. Human integrin $\alpha_v\beta_3$ is expressed on U87MG tumor cells (a human cancer cell line) while the tumor vasculature expresses mouse integrin $\alpha_v\beta_3$. As shown in Fig. S4a, Abegrin™ (anti-human integrin $\alpha_v\beta_3$ monoclonal antibody) staining afforded strong signal for U87MG tumor cells but not HT-29 tumor cells. No co-localization between Abegrin™ staining and CD31 staining was observed for either U87MG tumor or HT-29 tumor, suggesting the vessels in neither of the two tumors were stained by Abegrin™ as murine tumor vessels do not express human integrin $\alpha_v\beta_3$. In Fig.S4b, anti-mouse β_3 staining showed strong vessel staining for U87MG tumor but weak staining for HT-29 tumor. The good co-localization of CD31 and mouse β_3 staining indicates that the tumor vasculature expresses mouse integrin $\alpha_v\beta_3$, although the expression level is different in different tumors.

Taken together, Fig.S4 shows that U87MG tumor has high human integrin $\alpha_v\beta_3$ expression in tumor cells and mouse integrin $\alpha_v\beta_3$ expression on the tumor vasculature while HT-29 tumor has low integrin $\alpha_v\beta_3$ expression in both. Note that both mouse

integrin $\alpha_v\beta_3$ (expressed on tumor vasculature) and human integrin $\alpha_v\beta_3$ (expressed on U87MG cells) can be recognized by c(RGDyK).

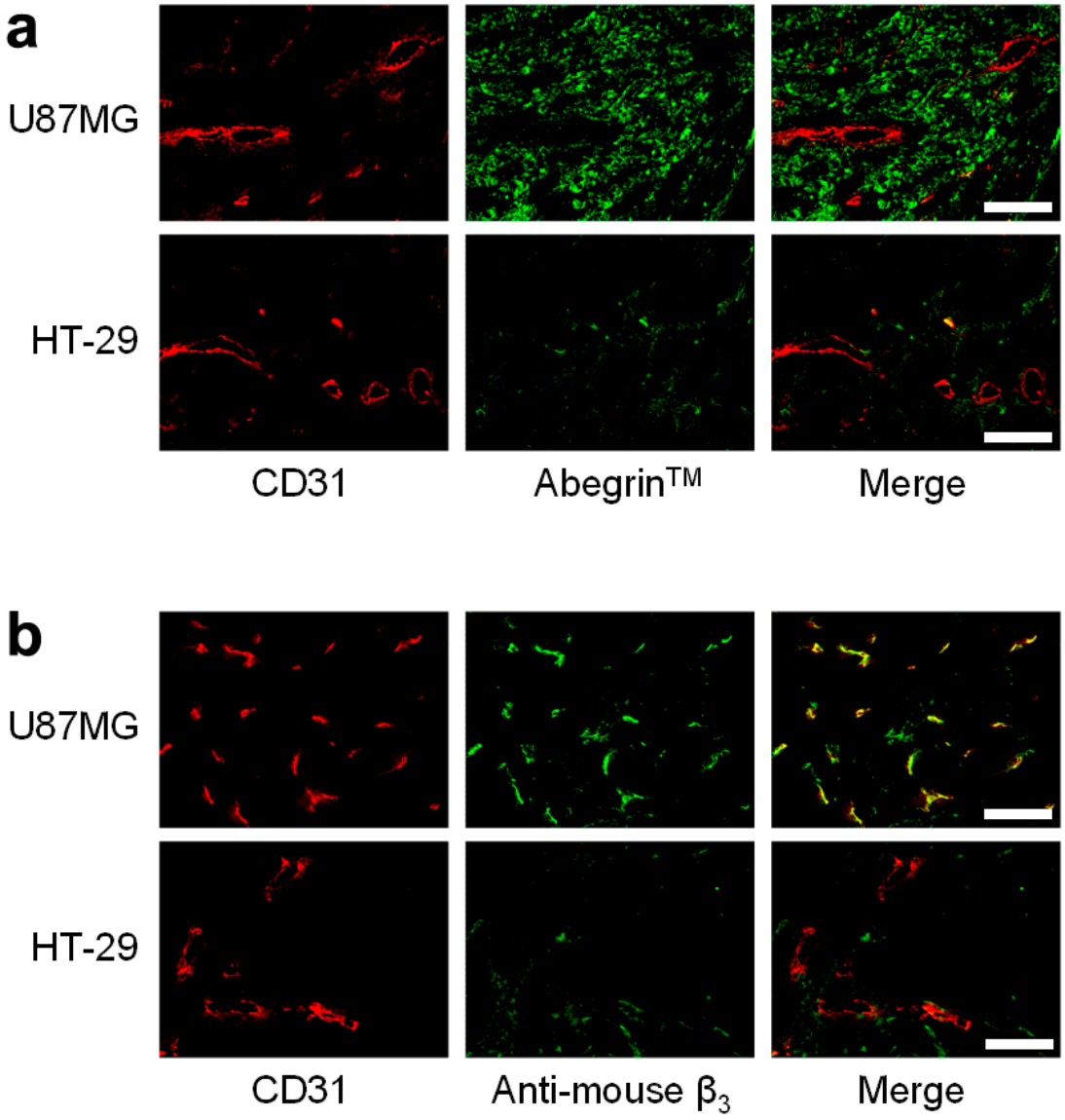

Fig. S5. Immunofluorescence staining of U87MG and HT-29 tumor sections. (a) CD31 and Abegrin™ (anti-human integrin $\alpha_v\beta_3$ monoclonal antibody) immunofluorescence staining showed that U87MG cells have much higher integrin $\alpha_v\beta_3$ expression than HT-29 cells. (b) CD31 and mouse β_3 staining of U87MG and HT-29 tumor sections revealed that U87MG tumor vessels also have higher integrin $\alpha_v\beta_3$ expression than HT-29 tumor vessels. Scale bar: 100 μm.

7. Raman measurement of SWNTs in tissues

SWNT solutions with known concentrations in a capilary glass tube were measured by Renishaw micro-Raman instrument (laser excitation wavelength = 785 nm). A glass capillary tube filled with SWNT solution was placed under the objective of the Raman microscope. After focusing at the center of the capillary, we recorded the Raman spectrum of the solution (100 mW power, 20 × objective, laser spot size ~3 × 60 μm^2, 10s collection time). Spectra were also taken by slightly changing the focus. The G band peak area was integrated from 1570 cm^{-1} to 1620 cm^{-1} and averaged for multiple spectra and then plotted against the concentrations of SWNTs (Fig. S6).

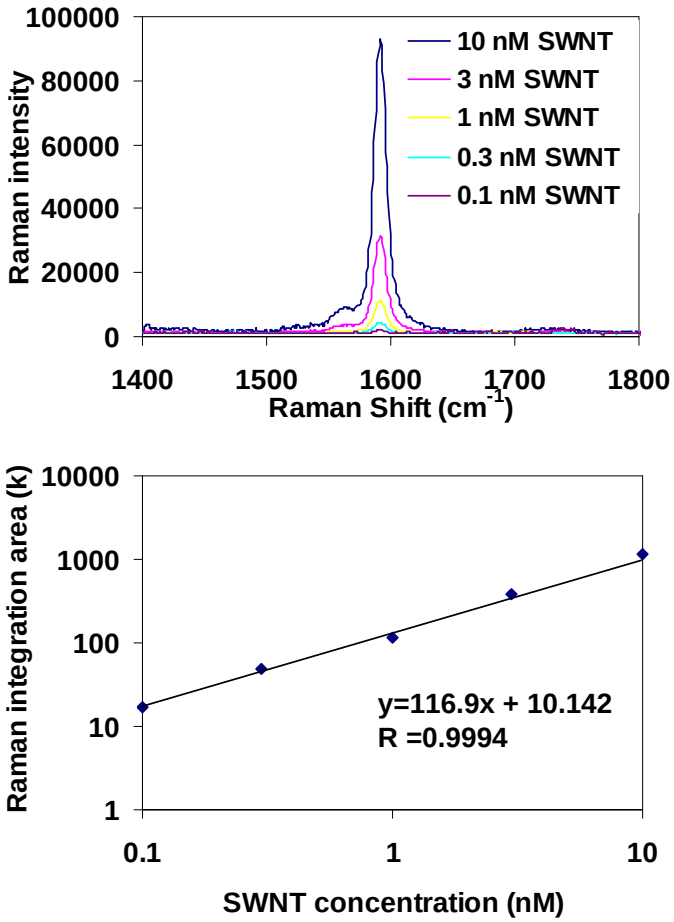

Fig. S6. Standard Raman calibration curve of SWNT solutions. (a) Raman spectra of SWNT solutions of different concentrations after subtracting background. (b) G-band intensity vs. SWNT concentration.

Raman spectra of tissue suspensions were collected similarly and the spectra were used to measure SWNT concentrations in the tissues against the standard calibration curve in Fig.S6. The Raman spectroscopy based %ID/g of SWNTs in a specific tissue was calculated by the following equation:

$$\%ID/g = \frac{([SWNT] \text{ in tissue suspension}) \times (\text{volume of tissue suspension})}{([SWNT] \text{ in injected solution}) \times (\text{volume of injected SWNT}) \times (\text{wet weight of tissue})}$$

References

1. Wang, H. F. et al. Biodistribution of carbon single-wall carbon nanotubes in mice. *J. Nanosci. Nanotechnol.* **4**, 1019 (2004).
2. Kam, N. W. S., O'Connell, M., Wisdom, J. A. & Dai, H. Carbon nanotubes as multifunctional biological transporters and near-infrared agents for selective cancer cell destruction. *Proc. Natl. Acad. Sci. USA* 102, 11600-11605 (**2005**).
3. Meares, C. F. et al. Conjugation of antibodies with bifunctional chelating agents isothiocyanate and bromoacetamide reagents methods of analysis and subsequent addition of metal ions. *Anal. Biochem.* **142**, 68 (1984).
4. Wu, Y., Cai, W. & Chen, X. Near-infrared fluorescence imaging of tumor integrin $\alpha_v\beta_3$ expression with Cy7-labeled RGD multimers. *Mol. Imaging Biol.* **8**, 226-236 (2006).